

# Ideal strength of random alloys from first-principles theory

Xiaoqing Li,<sup>1,\*</sup> Stephan Schönecker,<sup>1,†</sup> Jijun Zhao,<sup>2,3,‡</sup> Börje Johansson,<sup>1,4</sup> and Levente Vitos<sup>1,4,5</sup>

<sup>1</sup>*Applied Materials Physics, Department of Materials Science and Engineering,  
Royal Institute of Technology, Stockholm SE-10044, Sweden*

<sup>2</sup>*School of Physics and Optoelectronic Technology and College of Advanced Science and Technology,  
Dalian University of Technology, Dalian 116024, China*

<sup>3</sup>*Key Laboratory of Materials Modification by Laser,  
Electron, and Ion Beams (Dalian University of Technology),*

*Ministry of Education, Dalian 116024, People's Republic of China*

<sup>4</sup>*Department of Physics and Astronomy, Division of Materials Theory,  
Uppsala University, Box 516, SE-75120, Uppsala, Sweden*

<sup>5</sup>*Research Institute for Solid State Physics and Optics,  
Wigner Research Center for Physics, Budapest H-1525, P.O. Box 49, Hungary*

(Dated: June 5, 2019)

The all-electron exact muffin-tin orbitals method in combination with the coherent-potential approximation has been employed to investigate the ideal tensile strengths of elemental V, Mo solids and V- and Mo-based random solid solutions. The present ideal tensile strengths, calculated assuming isotropic Poisson contraction, are 16.1, 26.7 and 37.6 GPa for bcc V in the [001], [111] and [110] directions, respectively, and 26.7 GPa for bcc Mo in the [001] direction, which are all in good agreement with the available theoretical data. When a few percent Tc is introduced in Mo, it is found that the ideal strength decreases in the [001] direction. For the V-based alloys, Cr increases and Ti decreases the ideal tensile strength in all principal directions. Adding the same concentration of Cr and Ti to V leads to ternary alloys with similar ideal strength values as that of pure V. The alloying effects on the ideal strength is explained using the electronic band structure.

PACS numbers: 62.20.-x, 71.15.Nc, 71.20.Be, 71.23.-k

## I. INTRODUCTION

High strength and good ductility define the two most important mechanical properties of metallic structure materials.<sup>1</sup> In materials, strength is usually controlled by the occurrence of grain boundaries, cracks, dislocations and other micro-structural defects. If such defects were not present, the strength would be limited by the stress at which the lattice itself becomes unstable with respect to a homogeneous strain. This stress referred to as the ideal strength, is the possible maximum strength of an ideal single crystal. The ideal strength is an inherent property of a material which can offer insight into the correlation between the intrinsic chemical bonding and the crystal symmetry and has been accepted as an essential mechanical parameter of single crystal materials.<sup>2</sup>

The experimental data on ideal strength are rather limited, since it is difficult to measure the ideal strength using experimental tools. There are only few experimental data that were obtained from tensile tests for whiskers<sup>3</sup> and from nanoindentation experiments.<sup>4</sup> Recently, calculations of ideal strength became of great interest because they represent an upper bound to the strength of any real crystal on the attainable stress. The ideal strength may be calculated under special loading conditions: ideal strength in tension, e.g., for high symmetry directions of cubic crystals under uniaxial load, or ideal strength in shear, e.g., for common slip systems  $\langle 111 \rangle \{112\}$  and  $\langle 111 \rangle \{110\}$  in body-centered cubic (bcc) crystals.<sup>5,6</sup>

The ideal strength is one of few mechanical properties

that can be calculated from first principles. The ideal strength of refractory metals (such as Mo, Nb, V, and W), late transition metals (such as Cu, Pt and Au), elements crystallizing in the diamond structure (Si, Ge, and C) as well as some ordered alloys (TiAl and Ni<sub>3</sub>Al) have been extensively investigated.<sup>6-18</sup> For example, Luo *et al.*<sup>15</sup> and Nagasako *et al.*<sup>6</sup> focused on the ideal tensile strength (ITS) of the bcc metals Mo, Nb, and V in the  $\langle 001 \rangle$  directions. Accordingly, in all of them the deformation starts along the Bain path, but branches away onto an orthorhombic path before the face-centered cubic (fcc) point is reached. In Mo, this orthorhombic distortion does not influence the ITS; however, in Nb and V, the branching occurs before the maximum stress on the tetragonal deformation curve is reached and hence causes a significant decrease in the ITS. The stress-strain relations and the corresponding theoretical tensile strengths of ordered  $\gamma$ -TiAl ( $L1_0$  structure) alloy exhibit strong anisotropy in different crystalline directions originating from the structural anisotropy of  $\gamma$ -TiAl.<sup>12</sup> In spite of all these theoretical efforts, the first-principles description of the ITS in random solid solutions is rather limited. This is because the material strength is sensitive to their structure. The only attempt<sup>19</sup> employed the virtual crystal approximation (VCA) to study the ITS of the binary Ti-V for concentrations of Ti equal to and higher than 30 at.%. The results showed that the more the ITS is decreased the more Ti is present in the alloy.

Vanadium rich ternary V-Cr-Ti alloys are important candidate structure materials for the first-wall/blanket of future fusion reactors.<sup>20,21</sup> These V-based alloys exhibit

excellent mechanical properties, decent thermal creep behavior, high thermal conductivity, good resistance to irradiation-induced swelling and damage, and long operating lifetime in the fusion environment.<sup>20–25</sup> Considerable efforts have been made to find optimal V-based alloy compositions that can endure the extreme environment of fusion-reactors. The available experimental data indicates that reasonable properties can be achieved by introducing a few percent Ti and Cr into the V matrix.<sup>26</sup> Consequently, the ternary V-Cr-Ti system has attracted broad interest, and in particular the compositions with 0–15 at.% Cr and 0–20 at.% Ti have been intensively investigated.<sup>27–31</sup> To the best of our knowledge, most experimental efforts on V-Cr-Ti alloys have been devoted to the ductile-brittle transition temperature before and after irradiation, swelling properties, and impact toughness as a function of Cr and Ti contents.

As a promising structure material for fusion reactors, V-based alloys must not only withstand radiation damage but should also keep intrinsic mechanical properties and structural strength. Thus it is necessary to study fundamental mechanical properties, such as elastic properties, which were systematically investigated for  $V_{1-x-y}Cr_xTi_y$  random alloys ( $0 \leq x \leq 0.1$  and  $0 \leq y \leq 0.1$ ) in our former works.<sup>32,33</sup> The second-order elastic constants describe the mechanical properties of materials in the small deformation region, where the stress-strain relations are linear. The ideal strength describes the mechanical properties of the material beyond the elastic region, which is important during the alloy design.

In this work, we use the all-electron exact muffin-tin orbitals method (EMTO) in combination with the coherent-potential approximation (CPA) to investigate the ITS of bcc elemental V and Mo solids as well as  $Mo_{0.9}Tc_{0.1}$  and  $V_{1-x-y}Cr_xTi_y$  ( $0 \leq x + y \leq 0.1$ ) random alloys as a function of concentrations. For sake of simplicity, here we consider only the ideal tensile strength corresponding to isotropic Poisson contraction. However, the present approach can easily be generalized to account for shear instabilities as reported in the case of several elemental metals.<sup>6,15</sup> The primary purpose of our work is to give an account of the application of the EMTO method to the calculation of ITS in bcc nonmagnetic metals and random alloys. Second, we aim to provide a consistent theoretical guide to further optimization of the composition of V-based alloys for structure material applications.

The structure of the manuscript is as follows. In Section II, we describe the computation tool and all important numerical details. The results are presented and discussed in Section III. Here, first we assess the accuracy of our calculations by considering pure Mo and V. Then we study the effects of the alloying elements on the ideal strength of Mo-Tc and V-Ti-Cr alloys. We make use of band filling arguments, canonical band theory, and structural energy differences to explain the trend of the computed ideal strength of V-based alloys.

## II. COMPUTATIONAL METHOD

### A. Total energy calculation

The first-principle method used in this work is based on density functional theory (DFT)<sup>34</sup> formulated within the Perdew-Burke-Ernzerhof (PBE) generalized gradient approximation for the exchange-correlation functional.<sup>35</sup> The Kohn-Sham equations were solved using the EMTO method.<sup>36–38</sup> The problem of disorder was treated within the CPA and the total energy is computed via the full charge-density technique.<sup>39–42</sup>

The EMTO method is an improved screened Korringa-Kohn-Rostoker (KKR) method,<sup>36</sup> where the full potential is represented by overlapping muffin-tin potential spheres. Inside these spheres, the potential is spherically symmetric and constant in between. By using overlapping spheres, one describes more accurately the exact crystal potential compared to conventional muffin-tin or non-overlapping methods. Further details about the EMTO method and its self-consistent implementation can be found in previous works.<sup>36–38,41,42</sup> The accuracy of the EMTO method for the equation of state and elastic properties of metals and alloys has been demonstrated in a number of previous works.<sup>32,37,40,43–47</sup> However, to our knowledge, no CPA-based alloy theory has previously been employed in the ab initio determination of the ideal strength of random solid solutions. This may be ascribed to the limited accuracy of the classical CPA-based electronic structure methods for systems with reduced crystal symmetry. In this respect, the present work represents a pioneering demonstration of the EMTO-CPA approach in ideal strength calculations for random alloys.

### B. Ideal tensile strength calculations for bcc crystals

The first step in ITS calculations is to compute the equilibrium lattice constant of the material in the ground state structure. The present alloys adopt the bcc structure. In the second step, an uniaxial tensile strain  $\epsilon$  is applied along a specific crystalline direction which mimics a certain tensile stress  $\sigma$ . For each value of the strain, we relaxed the deformed structures under constraints described below to make sure that no internal forces remain in the crystal in directions perpendicular to the applied stress. From the above steps, we obtained energy versus strain curves and derived stress versus strain data. The first maximum on the stress-strain curve defines the ITS for the selected strain path.

The stress  $\sigma$  is given by<sup>16</sup>

$$\sigma(\epsilon) = \frac{1}{\Omega(\epsilon)} \frac{\partial E}{\partial \epsilon}, \quad (1)$$

where  $E$  is the total energy per atom and  $\Omega(\epsilon)$  is the volume per atom at a given tensile strain.  $\epsilon$  is the strain of

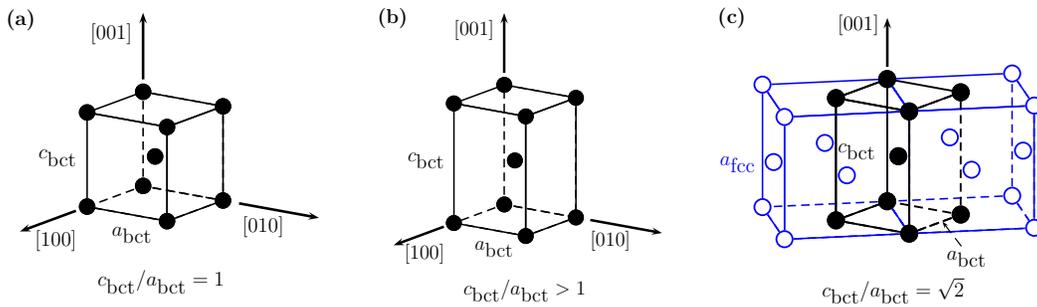


FIG. 1. (Color online) Illustration of the lattice distortion of the bcc structure due to an applied uniaxial stress in the [001] direction. (a) The unit cell in the absence of strain is bcc (in the bct delineation  $c_{\text{bcc}}/a_{\text{bcc}} = 1$ ). For finite strain, the lattice symmetry is initially distorted to bct (b) and becomes fcc for  $c_{\text{bcc}}/a_{\text{bcc}} = \sqrt{2}$  (c). In panel (c), two entire fcc conventional unit cells are drawn to ease its identification.

the simulation cell in the direction of the applied uniaxial force  $\hat{\mathbf{F}}$  and is defined as

$$\epsilon = \frac{l_{\parallel} - l_0}{l_0}, \quad (2)$$

where  $l_{\parallel}$  and  $l_0$  denote the length of the cell parallel to  $\hat{\mathbf{F}}$  in the final state and in the initial state (without any force), respectively. The initial state corresponds to the equilibrium bcc structure with energy  $E_0$ . We define the *uniaxial strain energy*  $\Delta E(l_{\parallel}, \hat{\mathbf{F}})$  following Ref. 48 as the total energy change upon deforming the material in the direction along the applied force, and relaxing with respect to the dimensions in the plane perpendicular to  $\hat{\mathbf{F}}$ , viz.

$$\Delta E(l_{\parallel}, \hat{\mathbf{F}}) = \min_{\mathbf{a}_1, \mathbf{a}_2} E(\mathbf{a}_1, \mathbf{a}_2, l_{\parallel}) - E_0. \quad (3)$$

The minimization is done with respect to the pair of unit cell vectors  $\{\mathbf{a}_1, \mathbf{a}_2\} \perp \hat{\mathbf{F}}$ .

In this work, we computed the ITS in the  $\langle 001 \rangle$ ,  $\langle 111 \rangle$  and  $\langle 110 \rangle$  directions of bcc elemental solids and alloys. Three different unit cell were employed to describe the distorted lattices since each direction breaks the symmetry of the bcc structure in a different way. First, we chose the [001] axis to be the direction of the applied force for  $\langle 001 \rangle$  ITS calculations. The symmetry of the bcc lattice is reduced to the body-centered tetragonal (bct) one, see Fig. 1, if the relaxation of the lattice is restricted to a change in length of the quadratic basal plane only. Accordingly, we may rewrite Eq. (3) with the in-plane lattice constant  $a_{\text{bcc}} \equiv a_1 = a_2$ ,  $a_i = |\mathbf{a}_i|$ , and  $\mathbf{a}_1 \cdot \mathbf{a}_2 = 0$ ,

$$\Delta E(c_{\text{bcc}}, [001]) = \min_{a_{\text{bcc}}} E(a_{\text{bcc}}, c_{\text{bcc}}) - E_0, \quad (4)$$

with  $c_{\text{bcc}} \equiv l_{\parallel}$  denoting the unit cell length along [001]. Increasing the axial ratio  $c_{\text{bcc}}/a_{\text{bcc}}$  from 1 to  $\sqrt{2}$  transforms the bcc lattice into the fcc lattice while the crystal remains bct during the transformation, see Fig. 1. This transformation corresponds to the Bain transformation<sup>49</sup>

and may occur under uniaxial loading environment.<sup>50</sup> Although the symmetry of the distorted lattice due to an uniaxial load along one of the high symmetry  $\langle 001 \rangle$  directions may be lower than tetragonal, e.g., orthorhombic if the relaxation is non-isotropic ( $a_1 \neq a_2$ ),<sup>2,15</sup> the bct symmetry is often maintained.<sup>14,16</sup> Since our aim is to compare the present results with previously published ones in order to establish the accuracy of the EMTO method for this type of calculations, here we did not consider lower symmetry than bct for the [001] calculations.

In an actual calculation of the stress-strain relation we selected a set of  $c_{\text{bcc}}$  values equidistantly separated by 2.2% of the bcc equilibrium lattice parameter corresponding to different strains  $\epsilon$ . For each value of  $c_{\text{bcc}}$  we computed the total energy on a dense mesh of  $a_{\text{bcc}}$  values to find the minimum according to Eq. (4). The total energies as well as the volume of each state of strain were fitted to polynomial fit functions and differentiated to obtain the stress as a function of strain (Eq. (1)). The maximum strain,  $\epsilon_m$ , is then the ITS at the maximum stress,  $\sigma_m$ . The choice of the order of the polynomial fit functions was crosschecked to avoid any substantial influence on the values of  $\sigma_m$  and of  $\epsilon_m$ . For consistency, we employed the same fit function for all types of distortion, i.e., along the  $\langle 001 \rangle$ ,  $\langle 111 \rangle$ , and  $\langle 110 \rangle$  directions.

Straining the bcc structure along the [110] axis reduces the lattice symmetry to face-centered orthorhombic (fco) symmetry, assuming that relaxation preserves the symmetry in the (110) plane. In the absence of strain, the fco lattice parameters,  $a_{\text{fco}}$ ,  $b_{\text{fco}}$ , and  $c_{\text{fco}}$ , fulfill  $a_{\text{fco}} = b_{\text{fco}} = \sqrt{2}c_{\text{fco}}$ , see Fig. 2 for a detailed illustration. Here, strain is applied to  $b_{\text{fco}} \equiv l_{\parallel}$  while  $a_{\text{fco}}$  and  $c_{\text{fco}}$  are relaxed keeping  $c_{\text{fco}}/a_{\text{fco}}$  fixed to the initial value of  $\sqrt{2}$  to make the computations feasible. We may hence write for the uniaxial strain energy of the [110] distortion,

$$\Delta E(b_{\text{fco}}, [110]) = \min_{a_{\text{fco}}} E(a_{\text{fco}}, b_{\text{fco}}) - E_0. \quad (5)$$

If an uniaxial strain is applied along the [111] direction parallel to the body diagonal of the bcc structure,

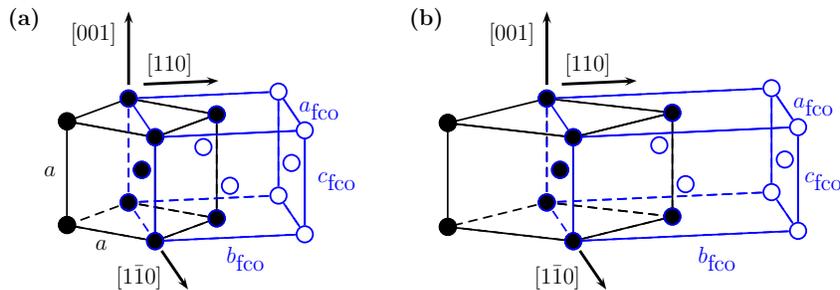


FIG. 2. (Color online) Illustration of the lattice distortion of the bcc structure due to an applied uniaxial stress in the  $[110]$  direction. (a) and (b) show the undistorted lattice and the distorted lattice, respectively. Both the fcc unit cell used in the computation and the (undistorted and distorted) bcc cell are sketched.

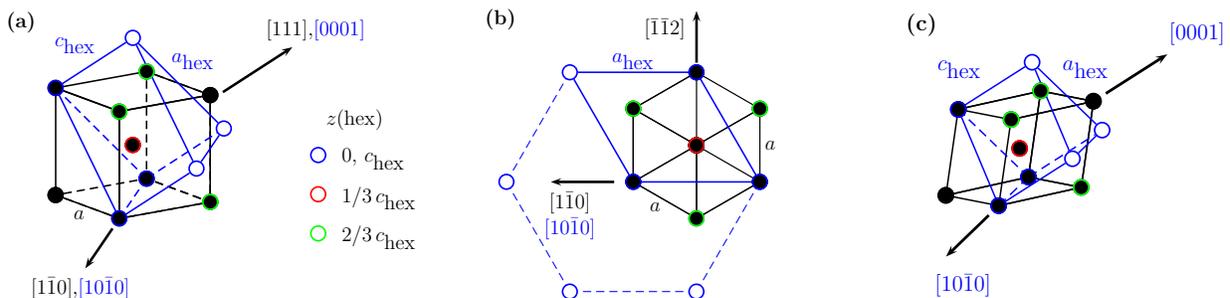


FIG. 3. (Color online) Illustration of the lattice distortion of the bcc structure due to an applied uniaxial stress in the  $[111]$  direction. (a) shows the undistorted bcc lattice with hexagonal delineation (a wedge representing one sixth of the conventional hex unit is drawn), the axial ratio is  $c_{\text{hex}}/a_{\text{hex}} = \sqrt{3}/8$ . The undistorted unit cell projected along  $[111]$  ( $[0001]$ ) is depicted in (b) to show more clearly the full symmetry of the hex lattice. A finite strain, (c), lowers the symmetry of the bcc lattice to a trigonal one.

the symmetry of the lattice is reduced to trigonal symmetry. The distorted lattice can be equivalently described by a hexagonal (hex) lattice or a rhombohedral lattice. Here, we chose the hex lattice, as sketched in Fig. 3. The  $[0001]$  axis and the  $[10\bar{1}0]$  axis of the hex lattice are oriented parallel to the  $[111]$  axis and the  $[1\bar{1}0]$  axis of the bcc lattice, respectively. In the absence of strain, the lattice parameters of the hex unit cell and the bcc cell are related by  $a_{\text{hex}} = \sqrt{2}a_{\text{bcc}}$  and  $c_{\text{hex}} = \sqrt{3}/4a_{\text{bcc}}$ , where  $a_{\text{hex}}$  denotes the in-plane lattice parameter of the hexagonal basal plane (the distance between two atoms of the smallest equal-sided triangle). The out-of-plane lattice parameter,  $c_{\text{hex}}$ , is oriented parallel to the threefold stacking axis. Bcc  $(111)$  planes are stacked along  $[0001]$  (ABCABC stacking) and two successive planes are displaced by  $1/3$  of  $c_{\text{hex}}$  (cf. Fig. 3). For each applied strain, interatomic distances in the  $(0001)$  planes are relaxed while the in-plane symmetry is preserved. The uniaxial strain energy relaxed with respect to  $a_{\text{hex}} \equiv a_1 = a_2$  becomes,

$$\Delta E(c_{\text{hex}}, [111]) = \min_{a_{\text{hex}}} E(a_{\text{hex}}, c_{\text{hex}}) - E_0. \quad (6)$$

When the hexagonal axial ratio  $c_{\text{hex}}/a_{\text{hex}}$  is identical to  $\sqrt{3}/2$  the strained hexagonal lattice coincides with the

simple cubic (sc) lattice. Similarly, when  $c_{\text{hex}}/a_{\text{hex}} = \sqrt{3}$  we recover the fcc lattice.

### III. RESULTS AND DISCUSSION

#### A. Equilibrium volume

The theoretical equilibrium lattice parameter of bcc Mo is  $3.165\text{\AA}$ , which agrees well with the experimental data<sup>51</sup>  $3.141\text{\AA}$ . When 10 at.% Tc is added into the Mo matrix, the lattice constants decreases from  $3.165\text{\AA}$  to  $3.156\text{\AA}$ . This trend can be understood by the smaller atomic radius of hexagonal close packed Tc ( $1.36\text{\AA}$ ) as compared to that of bcc Mo ( $1.40\text{\AA}$ ).<sup>51</sup>

Theoretical equilibrium lattice parameters and elastic properties of V and disordered V-Cr-Ti alloys were investigated with EMTO and the CPA in our previous paper, see Ref. 32. Since our employed lattice parameters are identical to these earlier results, we refer the reader to this reference for a detailed account of the numerical data. Here we only restate the most important findings necessary to follow the ongoing discussion.

For pure vanadium, the calculated equilibrium lattice

parameter is 2.998Å, in good agreement with the corresponding experimental value<sup>52</sup> 3.03 Å at low temperature. For V alloyed with Ti and Cr, we found that the theoretical lattice constants increase (decrease) with increasing Ti (Cr) concentrations, for instance, the lattice constant of the alloy with 10% Cr is 2.981 Å, but for the alloy with 10% Ti, the lattice constant is 3.021Å. Our theoretical results confirmed the experimental trend.<sup>53</sup>

Our results showed that the EMTO method with the CPA can be used to describe the elastic properties of V-based alloys and gave the accuracy and available results in the small deformation region. Since the ideal strength describes the mechanical properties of the material beyond the linear stress-strain response, the ideal strength is very important during the design process of alloys. Thus, based on the equilibrium lattices constants and energies that we obtained in our former calculations,<sup>32</sup> we calculated the ideal tensile strength of pure V, and investigated the ideal tensile strength of bcc nonmagnetic  $V_{1-x-y}Cr_xTi_y$  random alloys as a function of Cr and Ti ( $0 \leq x + y \leq 0.1$ ) concentrations using EMTO with the CPA.

### B. Ideal strength of pure vanadium and molybdenum

To assess reliability of our computational approach, we first performed the simulation of a tensile test in V for uniaxial loadings along the [001], [110] and [111] directions. The corresponding stresses as a function of strain are displayed in Fig. 4. Along the [001] direction, stress increases with increasing strain up to a maximum of  $\sigma_m = 16.1$  GPa at a strain of  $\epsilon_m = 16.0\%$ . Clearly different from the [001] direction are the much higher ideal stresses in the [111] direction and the [110] direction where the stress reaches a maximum of 26.7 GPa at  $\epsilon_m = 35.2\%$  and 37.6 GPa at  $\epsilon_m = 38.3\%$ , respectively.

In the inset of Fig. 4(a), we also show stress as a function of strain in the small deformation region ( $\epsilon \leq 0.5\%$ ). These strain-stress relations are linear and follow Hooke's law,  $\sigma = E \cdot \epsilon$ , where  $E$  is Young's modulus, which depends on the direction of the applied force.<sup>54</sup> For further use, the explicit expression of  $E$  in terms the cubic elastic constants ( $C_{11}$ ,  $C_{12}$ , and  $C_{44}$ ) for an uniaxial stress in  $\langle 001 \rangle$  directions ( $E_{\langle 001 \rangle}$ ) and in  $\langle 111 \rangle$  directions ( $E_{\langle 111 \rangle}$ ) are given by

$$E_{\langle 001 \rangle} = 6C' \cdot \frac{B}{C_{11} + C_{12}} \quad (7)$$

$$E_{\langle 111 \rangle} = 3C_{44} \cdot \frac{1}{1 + \frac{C_{44}}{3B}}, \quad (8)$$

where  $C' = (C_{11} - C_{12})/2$  and  $B = (C_{11} + 2C_{12})/3$  are the tetragonal shear elastic constant and the bulk modulus, respectively. According to Fig. 4(a) (inset), the [001] direction exhibits the largest Young's modulus, which means that the [001] direction is the strongest

direction among the three selected ones in the small deformation region, while the Young's moduli in the [110] and [111] directions are smaller and degenerate. Indeed, using the theoretical elastic parameters of bcc V<sup>32</sup> we obtain  $E_{\langle 001 \rangle} = 205.3$  GPa and  $E_{\langle 111 \rangle} = 101.4$  GPa. These values are in good agreement with those derived directly from Fig. 4(a) (approximately 200 GPa and 110 GPa for  $E_{\langle 001 \rangle}$  and  $E_{\langle 111 \rangle}$ , respectively). This behavior at small strains is distinct from the one for the larger, non-linear deformation region, where [110] ultimately replaces [001] as the strongest direction.

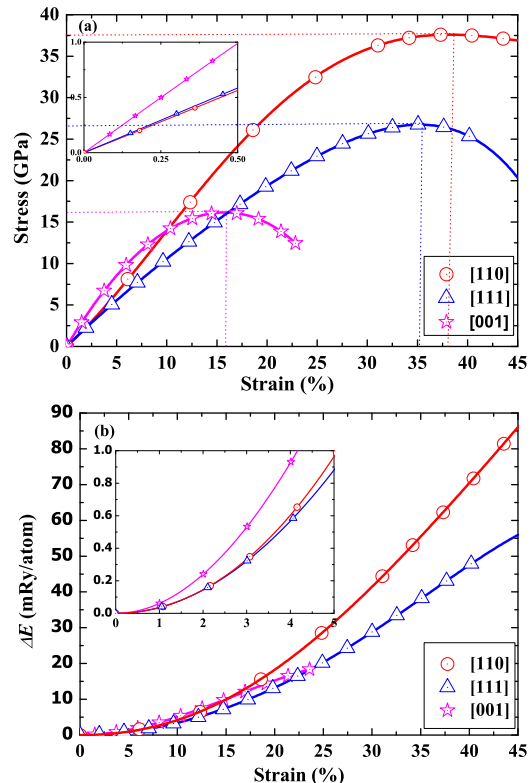


FIG. 4. (Color online) The ideal strength (a) and energy (b) of pure V in [001], [111] and [110] directions as a function of strain. The insets show the trends of ideal strength and energy in the smaller strain region.

The ideal tensile strength  $\sigma_m$  corresponding to the strain  $\epsilon_m$  from our and other calculations in [001], [111], and [110] directions for vanadium are listed in Table I. First, it can be seen that for the [001] direction, projector-augmented-wave (PAW) works<sup>55,56,58</sup> reported similar ideal strength values, such as Nagasako *et al.*<sup>6</sup> gave a value of  $\sigma_m = 17.8$  GPa at  $\epsilon_m = 17.0\%$  and Liu *et al.* reported a value of  $\sigma_m = 19.1$  GPa at  $\epsilon_m = 18.0\%$ . Our EMTO results for stress and strain are slightly smaller than the PAW values however still in good agreement. Li *et al.*<sup>19</sup> tabulated a value of  $\sigma_m = 16.8$  GPa at  $\epsilon_m = 16.0\%$  using pseudo potentials (PP). Our results are in agreement with their values. Krenn *et al.* obtained an ITS

TABLE I. The ideal tensile strength  $\sigma_m$  (GPa) and the corresponding strain  $\epsilon_m$  (%) from our and published computations in [001], [111], and [110] directions for a pure vanadium crystal and for the [001] direction of molybdenum.

element	method	direction/[001]		direction/[111]		direction/[110]	
		$\sigma_m$ (GPa)	$\epsilon_m$ (%)	$\sigma_m$ (GPa)	$\epsilon_m$ (%)	$\sigma_m$ (GPa)	$\epsilon_m$ (%)
V	EMTO	16.1	16.0	26.7	35.2	37.6	38.3
	PAW Ref. 55	19.1	18.0	31.0	36.0	32.8	42.0
	PAW Ref. 6	17.8	17.0				
	PAW Ref. 56	18.9	18.2				
	PP Ref. 19	16.7	16.0				
	PP Ref. 17	12.2	8.3				
Mo	EMTO	26.7	12.0				
	FP-LAPW Ref. 57	25.4	10.0				
	PP Ref. 15	28.8	13.0				

value of 12.2 GPa at an attainable strain of 8.3%, which is considerably lower compared with all other theoretical results. The difference may be due to their estimation of the ideal stress assuming a sinusoidal stress-strain relation on the basis of Frenkel's<sup>59</sup> and Orowan's<sup>60</sup> works.

Comparing the ITSs in [001], [111] and [110] directions among each other, we identify the [001] direction as the weakest one. We note that earlier ab initio approaches<sup>2,8,15,16,18,61–63</sup> consistently identified the  $\langle 001 \rangle$  directions as the weak directions in tension for elements crystallizing in the bcc structure. The ITSs of V along the [111] and [110] directions are clearly larger than the one along [001], the ideal strength along the [110] direction exhibiting the largest value. Černý and Pokluda<sup>18,63</sup> have investigated various bcc transition metals and also predicted the largest stresses for the  $\langle 110 \rangle$  directions.

Our computed maximum stress for the [110] direction is larger than the only other available theoretical data, Ref. 55, which may be attributed to our constraint relaxation (fixed lattice parameter ratio  $c_{fco}/a_{fco} = \sqrt{2}$ ). If this constraint is released as done in Ref. 55, the total energy for each lattice distortion may be lowered and hence the uniaxial strain-energy curve may be shallower compared to a constraint calculation which eventually lowers the ideal strength for the [110] direction.

The ideal stress of V in the  $\langle 111 \rangle$  directions is significantly larger than the stress in the  $\langle 001 \rangle$  directions. This may easily be understood on the basis of structural energy differences<sup>64,65</sup> (SEDs) as outlined in the following. The stability of a crystal structure relative to another one for one and the same element/alloy may be expressed in terms of their mutual energy difference, or often referred to as SED. We at first note that the total energy versus strain curve of the strain in [111] direction raises stronger than the other ones in the range given (the corresponding [001] curve even flattens), see Fig. 4. The distorted bct lattice of the [001] deformation and the distorted hex lattice of the [111] deformation coincide with the fcc lattice (at  $c_{bct}/a_{bct} = \sqrt{2}$ ) and with the sc lattice

(at  $c_{hex}/a_{hex} = \sqrt{3/2}$ ), respectively. All cubic Bravais lattices are symmetry dictated maxima of the respective energy versus strain curves,<sup>66–69</sup> i.e., the uniaxial strain energy *must level off* to the fcc-bcc structural energy difference and to the sc-bcc structural energy difference for an elongation along [001] and an elongation along [111], respectively, albeit at strains larger than the maximum strain ( $\epsilon_m$ ). This implies a limitation on the maximum stress since it restricts the uniaxial strain energy ( $\Delta E$ ) to the structural energy differences within the strain interval ( $\Delta\epsilon$ ) to accomplish the transformation from bcc to either fcc or sc, i.e., the ratio  $\Delta E/\Delta\epsilon$  is bounded. We argue that the maximum stress can be estimated from the previous bound on the basis of SEDs which then allows to understand the anisotropy of the attainable maximum stress with respect to uniaxial forces applied in certain crystallographic directions.

For a more quantitative analysis, we below assume a state of strain with constant volume fixed to the theoretical bcc equilibrium volume per atom,  $\Omega_{bcc}$ . This is to keep the presented argument both simple and general, and is neither a severe approximation since the relaxed volumes of all three cubic structures of V, i.e., the volumes of the initial and final states of the transformation, differ from another by less than 6%. We then may approximate the “true”  $\sigma_m$  by rewriting Eq. (1),

$$\sigma_m \approx \sigma_m^{\text{SED}} = \frac{1}{\Omega_{bcc}} \frac{\Delta E}{\Delta\epsilon}, \quad (9)$$

where  $\Delta E$  is either the fcc-bcc or the sc-bcc structural energy difference, and  $\Delta\epsilon$  is the strain at constant volume necessary to transform the bcc lattice into either the fcc lattice or into the sc lattice. Readily one may find,  $\Delta\epsilon_{[001]} = (1 - 0.5^{1/3})/0.5^{1/3} \approx 0.260$  and  $\Delta\epsilon_{[111]} = (1 - 0.25^{1/3})/0.25^{1/3} \approx 0.587$  for the [001] distortion and the [111] distortion, respectively. We computed for V  $\Delta E \equiv E_{fcc} - E_{bcc} = 20.48\text{mRy/atom}$  and  $\Delta E \equiv E_{sc} - E_{bcc} = 82.76\text{mRy/atom}$ . Using  $\Omega_{bcc} = 13.4695 \text{ \AA}^3$  and Eq. (9), the above SEDs yield  $\sigma_m^{\text{SED}} = 12.8 \text{ GPa}$  and  $\sigma_m^{\text{SED}} = 22.9 \text{ GPa}$  for the [001] distortion and the [111]

distortion, respectively. These simple estimates are to be compared to our ab initio results (Table I), where we obtained 16.1 GPa and 26.7 GPa for the respective ideal stresses. Thus, the anisotropy of the ideal stress may indeed<sup>68</sup> be understood on the basis of SEDs, if the uniaxial strain energy exhibits nearby symmetry dictated maxima.

The just presented argument, however, can not be used to explain the relative magnitude of  $\sigma_m$  for uniaxial loading in the  $\langle 110 \rangle$  directions of the bcc lattice, because the distorted orthorhombic lattice (Fig. 2) does not coincide with a higher symmetric one for any value of the strain  $\epsilon > 0$ , i.e., the uniaxial strain energy does not level off as if there is a nearby symmetry dictated extremum. It was pointed out<sup>70</sup> that such extrema can be created if the transformation path includes an identical structure related to the original one by shear, rotation or alternate structures which are connected to the original one by a structural phase transformation.

To further assess the accuracy of our computational approach, we calculated the ITS of bcc molybdenum. Since the [001] direction was already identified to be the weakest direction of bcc Mo, we here concentrated on this direction only. The ideal strength of solid Mo obtained in this work and previously published results are shown in Table I. One can see that our present results are very close to the other theoretical evaluations. In detail, the EMTO ideal strength reads 26.7 GPa at  $\epsilon_m=12.0\%$ . Joshi *et al.*<sup>57</sup> obtained for the stress and the corresponding strain 25.4 GPa and 10%, respectively, using the full potential linearized augmented plane wave method (FP-LAPW).

Based on the above findings, we conclude that our theoretical tool is able to describe the ideal strength of the V and Mo systems with sufficiently high accuracy and thus can be further employed to study V- and Mo- based alloys.

### C. Poisson ratio

In the following structural analysis, we investigate the volume-strain dependence for applied stress in the [001] direction and relate it to the tetragonal Poisson ratio. We define the tetragonal, i.e., strain dependent, Poisson ratio,  $\nu(\epsilon)$ , as the negative of the derivative of the length normal to the applied force with respect to the length of the cell in the direction of the applied force, viz.

$$\nu(\epsilon) \stackrel{\text{def}}{=} -\frac{da_{\text{bct}}(\epsilon)}{dc_{\text{bct}}(\epsilon)}. \quad (10)$$

Figure 5 depicts the strain dependence of the volume and the tetragonal Poisson ratio for both V and Mo. When  $\epsilon$  goes to zero, the present Poisson ratio should reduce to the cubic Poisson ratio along the [001] direction. For the present metals, the experimental cubic Poisson ratios are 0.258<sup>71</sup> and 0.338<sup>72</sup> for Mo and V, respectively. The cubic Poisson ratios according to Fig. 5 are 0.20 and

0.32 for Mo and V, respectively, which are close to the experimental data.

From Eq. (10), one may readily obtain the following relation for the stationary state of the volume change with strain,  $d\Omega(\epsilon)/d\epsilon|_{\epsilon_i} = 0$ ,

$$\nu_i = \frac{a_{\text{bct}}(\epsilon_i)}{2c_{\text{bct}}(\epsilon_i)} = \frac{1}{2} \sqrt{\frac{\Omega(\epsilon_i)}{\Omega_{\text{bcc}}(1 + \epsilon_i)^3}}, \quad (11)$$

where  $\nu_i$  is the tetragonal Poisson ratio at which the volume change is zero. In response to the applied strain, the volume increases up to a critical strain ( $\epsilon_i$ ) of approximately 15% and 20% for Mo and V, respectively. The volume change at the critical strain is zero, and becomes negative for strains larger than the critical strain. The critical strains of Mo and V are larger than their ideal strains. From Fig. 5, we identify the critical Poisson ratios  $\nu_i(\text{Mo}) = 0.41$  and  $\nu_i(\text{V}) = 0.39$ . These critical Poisson ratios occur at axial ratios  $c_{\text{bct}}/a_{\text{bct}}(\text{Mo})=1.22$  and  $c_{\text{bct}}/a_{\text{bct}}(\text{V})=1.28$  (cf. Eq. (11)).

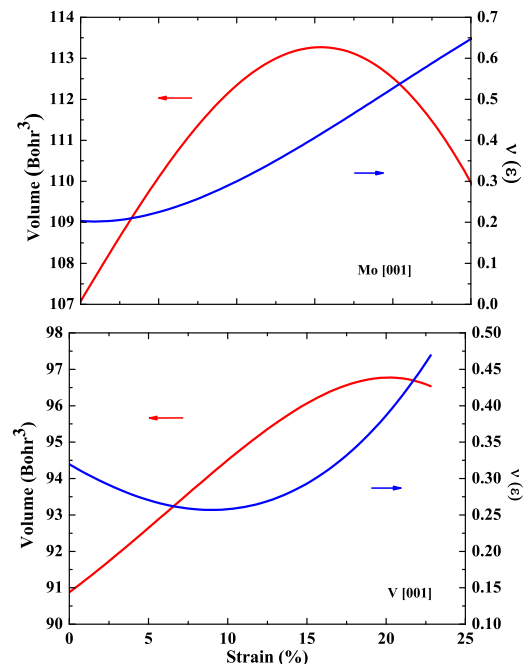


FIG. 5. (Color online) The atomic volume and the tetragonal Poisson ratio of V and Mo as a function of strain in the [001] direction.

### D. Ideal strength of molybdenum-technetium alloy

Next, we investigated the alloying effect of technetium on the ideal strength of bcc molybdenum-technetium alloys in the concentration range up to 10 at.% Tc along the [001] direction. The stress-strain dependence for Mo-Tc alloys is displayed in Fig. 6 and the corresponding

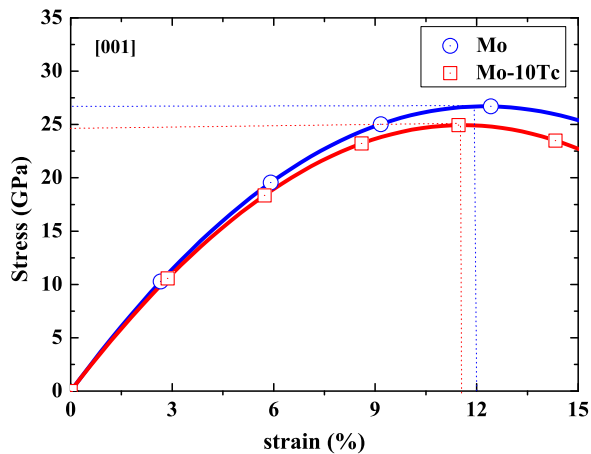


FIG. 6. (Color online) The ideal tensile strengths of Mo single crystal and the Mo-10Tc alloy as a function of strain in the [001] direction.

data are listed in Table II. From Fig. 6, we identify  $\sigma_m = 24.9$  GPa at  $\epsilon = 11.6\%$  for the Mo-10Tc alloy. Compared to pure Mo, Tc decreases the ideal strength. Bcc Mo has a  $d$ -band occupation of approximately 4.6 electrons as obtained from our EMTO calculation. According to band filling theory and DFT calculations,<sup>64,69</sup> the fcc-bcc SED of Tc is smaller than the one of Mo which means a destabilization of the bcc structure with respect to the fcc structure. Thus, based on Eq. (9), the ideal strength of Mo-Tc should be smaller than that of Mo, in line with the results from Fig. 6.

### E. Ideal strength of V-based alloys

In the following we turn to the V-based alloys and investigated the effect of the alloying elements Cr and Ti on the ITS of bcc V. The total concentration of both solutes was varied in the range from 0 to 10%. Figure 7 shows the composition dependence of the ideal strength of ternary bcc V-Cr-Ti random alloys along the [001], [111], and [110] directions and the corresponding numerical data for selected compositions are listed in Table II. From Fig. 7, it can be clearly seen that the ideal strengths of the vanadium binary alloy for all directions increase with increasing Cr content and decrease with Ti addition into pure V. For instance along the [001] direction, an addition of 5% Ti to V reduces the ITS by 1.2 GPa, i.e., from 16.1 GPa to 14.9 GPa. If however 5% Cr are added to the V matrix, the ITS increases by the same amount to 17.3 GPa.

Li *et al.*<sup>19</sup> calculated the ideal strength of Ti-V alloys for concentrations of Ti  $\geq 30$  at.% based on a PP method and the VCA. Their results confirm our trend, namely that the more Ti is present in the alloy the more the ideal strength is decreased. To further assess our results, we also calculated the ITS of the V-30Ti alloy. Our value

of 9.4 GPa is close to the 10 GPa obtained by Li *et al.*<sup>19</sup> for the same alloy composition. More importantly, the alloying effect obtained by Li *et al.* is  $-6.7$  GPa/30%Ti, which is in perfect agreement with the one obtained by us.

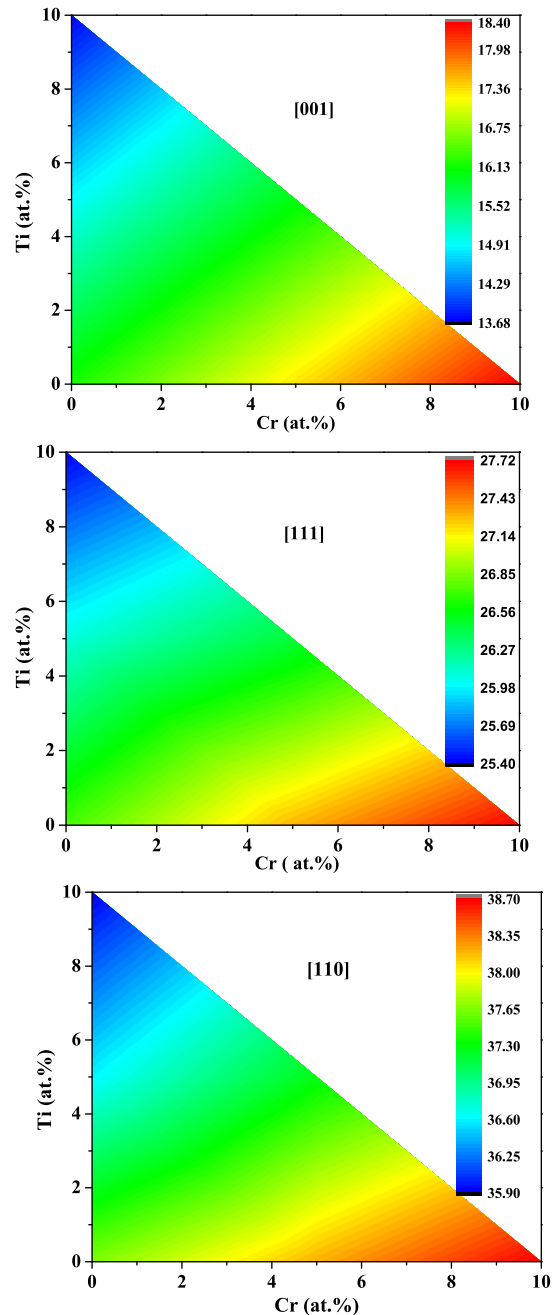


FIG. 7. (Color online) The ideal strength of V-based alloys in [001], [111] and [110] directions as a function of Cr and Ti. All stress values are in GPa.

The addition of chromium or titanium into the vanadium matrix leads to opposite consequences for the ideal strength of binary vanadium alloys. It is apparent from our data, that the effect of both elements on  $\sigma_m$  is how-

TABLE II. The ideal tensile strength  $\sigma_m$  (GPa), corresponding strain  $\epsilon_m$  from our calculations in [001], [111] and [110] directions for vanadium-based alloys and [001] for Molybdenum-10%Technetium alloy.

composition	direction/[001]		direction/[111]		direction/[110]	
	$\sigma_m$ (GPa)	$\epsilon_m$ (%)	$\sigma_m$ (GPa)	$\epsilon_m$ (%)	$\sigma_m$ (GPa)	$\epsilon_m$ (%)
V-10Cr	18.4	16.2	27.7	34.3	38.7	37.6
V-5Cr	17.3	16.1	27.3	34.4	38.2	38.0
V	16.1	16.0	26.7	35.2	37.6	38.3
V-5Cr-5Ti	16.0	16.0	26.5	35.3	37.3	38.2
V-5Ti	14.9	15.3	26.1	35.2	36.6	38.5
V-10Ti	13.7	15.2	25.4	35.3	35.9	38.3
Mo-10Tc	24.9	11.6				

ever of similar magnitude. As a result of both the opposite alloying effect and their similar order,  $\sigma_m$  is almost unchanged if equal amounts of Cr and Ti are alloyed to V. Hence, equi-composition V-Ti-Cr alloys possess nearly the same ideal strength as pure vanadium (equi-composition alloys are situated along the diagonal in Fig. 7). For example, the ideal strength of V-5Cr-5Ti is 16.0 GPa, which is very close to the 16.1 GPa for the pure V solid.

Furthermore from our data in Table II, we infer that the [001] direction exhibits the lowest maximum strain value among all three directions. The ratio of the calculated maximum strain along the [111] direction to the calculated maximum strain along the [001] direction for all alloys varies from 2.11 to 2.32. That seems plausible since the strain at constant volume necessary to transform the bcc lattice into the sc lattice ( $\Delta\epsilon_{[111]}$ ) is much larger than the strain necessary to transform the bcc lattice into the fcc lattice ( $\Delta\epsilon_{[001]}$ ), cf. Sec. III B, in fact their ratio is 2.260. This agreement may however be fortunate. It is obvious that the “true”  $\epsilon_m$  is much smaller than  $\Delta\epsilon$ , since the uniaxial strain energy levels off around the stable bcc state and around the fcc and sc extrema. If this leveling off is presumably symmetric on the minimum and the maximum in energy then  $\epsilon_m$  is roughly  $\Delta\epsilon/2$  for the respective directions, which however preserves their mutual ratio (2.260). We further observe from our data in Table II, that the strain maximum for the [001] distortion slightly increases (decreases) with increasing Cr (Ti) amount in the binary alloy. The equi-composition alloy V-5Cr-5Ti has the same data as pure V.

A direct comparison of the theoretical ITS with the engineering strength is not possible, since the latter is determined by the dislocation network whereas the prior is a simple measure of the strength of the chemical bonds for an ideal crystal. The present calculations indicate that the ITS of V decreases with Ti and increases with Cr. The ultimate tensile strengths of V- $x$ Cr-(4-5)Ti ( $0 \leq x \leq 15$ ) polycrystalline alloys have been measured in the temperature range from room temperature to about 1000K by Chuang *et al.*<sup>20</sup> For all measurements, the ultimate tensile strength increased monotonically with increased Cr content, which agrees well with the present trend ob-

tained for ITS. On the other hand, the yield strength of Ti-alloyed V increases with the amount of Ti,<sup>73</sup> which is opposite to the trend obtained for the present ITS.

### F. Electronic structure and ideal strength

The ideal strength of materials is ultimately due to the atomic bonding strength. It is well established<sup>74-76</sup> that the electronic structure and the bonding in transition metals is governed by a narrow valence  $d$ -band that hybridizes with a broader valence nearly-free-electron  $sp$ -band. SEDs for the transition metal series (disregarding the effect of magnetism in the present discussion) that give rise to the experimentally observed sequence of stable crystal structures are well understood in terms of band filling within this band picture.<sup>64,65,77</sup> It is clear that mainly the gradual filling of the  $d$ -band not only dictates crystal structure sequences in all three transition metal series, but also trends of the equilibrium volume dependence,<sup>76,78</sup> the cohesive energy,<sup>77-79</sup> the bulk modulus,<sup>80</sup> and elastic constants.<sup>81,82</sup> Here we argue that the observed trend of  $\sigma_m$  for V-Cr-Ti alloys may as well be understood on the basis of band filling arguments.

Figure 8 shows the density of states (DOS) of pure V, vanadium alloyed with 10% Cr and with 10% Ti, as well as the DOS of the equi-composition V-5Cr-5Ti alloy as obtained from our CPA calculations. We notice that the curves of V-10Cr and of V-10Ti are almost rigidly shifted with respect to the one of V, while the shape of their DOSs is merely effected by alloying vanadium with adjacent elements in the periodic table. This rigid band shift behavior signals an increase of the  $d$ -occupation (increase of the number of valence electrons) and a decrease of the number of  $d$ -occupation (decrease of the number of valence electrons) for Cr addition and Ti addition, respectively. Thus, alloying V with Cr and Ti changes the band filling. The DOS of V-5Cr-5Ti is virtually not shifted with respect to the one of V which indicates a zero net gain in the number of  $d$ -electrons in the matrix.

Since the band filling is the most important parameter determining structural stability in transition metals, it is straightforward to correlate the  $d$ -band filling due to

alloying to the ideal stress via SEDs in a manner similar to our approach in Sec. III B. For the refractory element V with a  $d$ -band occupation of approximately four electrons, we expect an increase of the fcc-bcc SED if more electrons are added into the  $d$ -band since the fcc-bcc SED of Cr is larger than the one of V.<sup>64,65,69</sup> That is, the SEDs corresponding to intermediate band fillings are simply assumed to lie in between the values of adjacent elements, corroborated by results of canonical band theory.<sup>64,83</sup> In other words, adding electrons starting at the band filling corresponding to the one of V stabilizes the bcc structure with respect to the fcc structure. The opposite holds for Ti alloying: the fcc-bcc SED of Ti is smaller than the one of V which means a destabilization of the bcc structure with respect to the fcc structure if electrons are removed from the  $d$ -band. Figure 9 displays the uniaxial strain energy as a function of strain for V based alloys in [001] direction. It is apparent that with respect to the curve of V, the strain curve rises more rapidly with increasing Cr concentration and falls with increasing Ti concentration. Furthermore, the energy-strain curve of the equi-composition alloy (V-5Cr-5Ti) is similar to that of V. Based on the above trends and according to the behavior of SEDs with band filling, we expect that the ideal strength in the [001] direction increases (decreases) with increasing Cr (Ti) concentration. To the best of our knowledge, sc-bcc SEDs for 3d transition metals have not been systematically investigated so far apart from the FM elements Fe, Co, and Ni,<sup>84</sup> and Cu.<sup>85</sup> From the trend of the sc-bcc SEDs we may however deduce the behavior of  $\sigma_m$  along the [111] direction as a function of band filling.

To confirm our expectation, we computed SEDs of vanadium based alloys and present the results in Table III. Following the same reasoning as in Sec. III B, we also computed  $\sigma_m^{\text{SED}}$  according to Eq. (9) employing the theoretical equilibrium volumes of these bcc alloys that we reported prior.<sup>32</sup> Note that the influence of the volume change due to alloying (which enters Eq. (9)) is about 2% and is not primarily responsible for the observed trend of  $\sigma_m$  since the volume effect is much smaller than the effect of  $\Delta E$ .

TABLE III. Structural energy differences (in mRy) of the fcc and the sc structure with respect to the stable bcc phase for bcc  $V_{1-x-y}Cr_xTi_y$  random alloys. Based on these energy differences and volumes from Ref. 32, the ideal strength  $\sigma_m^{\text{SED}}$  (in GPa) is approximated according to Eq. (9).

composition	direction/[001]		direction/[111]	
	$E_{\text{fcc}} - E_{\text{bcc}}$	$\sigma_m^{\text{SED}}$	$E_{\text{sc}} - E_{\text{bcc}}$	$\sigma_m^{\text{SED}}$
V-10Cr	23.00	14.6	84.79	23.9
V-5Cr	21.74	13.7	83.99	23.5
V	20.48	12.8	82.76	22.9
V-5Cr-5Ti	20.28	12.6	82.76	22.8
V-5Ti	19.06	11.8	81.98	22.4
V-10Ti	17.63	10.8	80.81	21.9

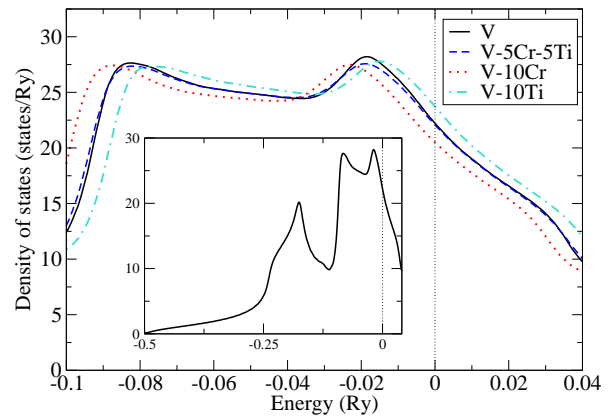


FIG. 8. (Color online) The DOSs of V-based alloys show that alloying with a single element leads mainly to a rigid band shift of the DOS. The inset displays the complete valence band of pure V. Energies are given relative to the Fermi level which is indicated by a vertical dotted line.

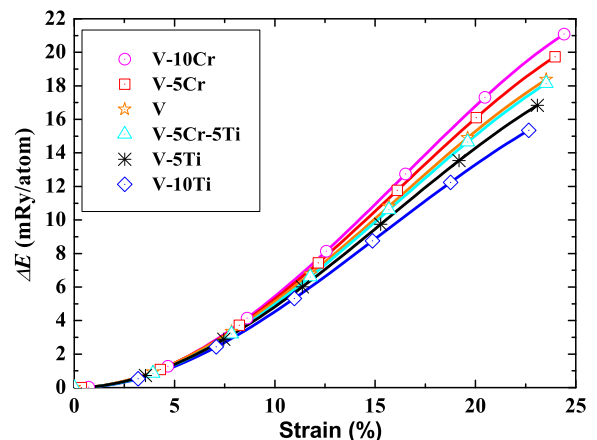


FIG. 9. (Color online) The uniaxial strain energy of V-based alloys for an applied strain in the [001] direction. The higher the 3d-band occupation is the steeper the curve progression is.

Our calculated SEDs clearly substantiate an increase of  $E_{\text{fcc}} - E_{\text{bcc}}$  with Cr addition, while the opposite effect is observed upon alloying with Ti. The function  $E_{\text{sc}} - E_{\text{bcc}}$  follows the same trend. On the basis of our simple estimate of the ideal strength (Table III), we conclude with respect to bulk V an increase of  $\sigma_m$  for the V-Cr binary alloys and a reduction of the ideal strength in case of V-Ti binary alloys. Our data affirms the larger relative change of  $\sigma_m$  for the [001] direction compared with the relative change of  $\sigma_m$  for the [111] direction. We find for the equi-composition alloy V-5Cr-5Ti, that its ideal strength almost retains the ideal strength of pure V.

Here we would like to bring up an interesting and important detail related to the above correlations. For the [001] distortions in V-Cr-Ti alloys, it is found that the composition dependence of the ideal strength correlates

well with that of the SEDs and also with the one followed by  $E_{\langle 001 \rangle}$ , which is ultimately determined by the composition dependence of  $C'$ .<sup>32</sup> However, for the [111] distortions, the ideal strength vs. SED correlation is not followed by the  $E_{\langle 111 \rangle}$ . For instance, Cr increases the [111] ideal strength and the sc-bcc energy difference, but slightly decreases  $E_{\langle 111 \rangle}$  and  $C_{44}$ . In other words, the present results confirm the often quoted  $C'$  vs. fcc-bcc energy difference correlation.<sup>81,82</sup> However, no such correlation seems to be valid between the  $C_{44}$  (or  $E_{\langle 111 \rangle}$ ) and the sc-bcc energy difference.

#### IV. CONCLUSIONS

Using the EMTO method in combination with the CPA, we have investigated the ideal strength of bcc V-based alloys in the [001], [110], and [111] directions and of Mo in the [001] direction. All ideal strengths considered here correspond to isotropic Poisson contraction, viz. no shape change was allowed perpendicular to the uniaxial stress. The present computed values for both V and Mo are in good agreement with previous calculations and thus confirm that our methodology has the accuracy needed for such kind of calculations.

For Mo-Tc random alloy, we have found that adding Tc to Mo decreases its ITS. In the case of V-based alloys, we have obtained that Cr addition increases and Ti addition decreases the ideal strength of bcc V in all three crystallographic directions. As a consequence, the ideal strength of V-Cr-Ti alloys remains virtually unchanged if equal amounts of Cr and Ti are introduced into the V host. We have shown that the observed alloying effects on the ideal strength can be understood on the basis of band filling arguments and structural energy differences.

The strength of a material in the range of validity of Hooke's law is characterized by its elastic constants. In our previous paper,<sup>32</sup> we investigated the strengthening effects of Cr and Ti on the elastic constants of disordered V-Cr-Ti alloys and found that Cr increases the tetragonal shear modulus ( $C'$ ) and Ti decreases it, while alloys with equi-concentrations have similar  $C'$  values as the elemental V. The effects of Cr and Ti on the  $C_{44}$  elastic constant of V are somewhat smaller (and have opposite signs) compare to those obtained for  $C'$ . On this ground,

combining our findings for the elastic regime and those obtained in this work for the ideal strength of V-Cr-Ti ternary alloys, we conclude that Cr strengthens the ITS and  $C'$  of these V-based alloys and Ti has a weakening effect on both ITS and  $C'$ . Furthermore, it is known,<sup>81,82</sup> that the  $E_{\text{fcc}} - E_{\text{bcc}}$  SEDs in nonmagnetic transition metals scale with their  $C'$ . This relation can now be extended to our vanadium alloys: an increase of the  $d$ -band filling by alloying Cr to V leads to increasing  $C'$  and ideal stress along the [001] direction, which scales with the corresponding SED. The effect of adding Ti to the V matrix (decrease of the  $d$ -band filling) is opposite to that of Cr addition on both  $C'$  and  $\sigma_m$ . We have shown that no similar correlation between  $C_{44}$ , ideal strength and sc-bcc structural energy difference can be established for the [111] mode.

The present results offer a consistent starting point for further theoretical modeling of the micro-mechanical properties of technologically important transition metal alloys. Based on these achievements, we conclude that the EMTO-CPA approach provides an efficient and accurate theoretical tool to design the mechanical strength of non-magnetic bcc random solid solutions and reveal the composition dependence of this fundamental physical parameter. Nevertheless, in such applications one should always monitor the basic muffin-tin and single-site CPA errors and make sure that they remain at acceptable level as a function of the lattice distortion and chemical composition. The extension of the present investigation to the case of magnetic alloys (such as the stainless steels) and to other Bravais lattices is in progress.

#### V. ACKNOWLEDGEMENTS

The Swedish Research Council, the Swedish Steel Producers' Association, the European Research Council, the China Scholarship Council and the Hungarian Scientific Research Fund (research project OTKA 84078), and the National Magnetic Confinement Fusion Program of China (2011GB108007) are acknowledged for financial support. S.S. gratefully acknowledges the Carl Tryggers Stiftelse för Vetenskaplig Forskning and Olle Erikssons stiftelse för materialteknik.

\* xiaoqli@kth.se

† stesch@kth.se

‡ zhaojj@dlut.edu.cn

<sup>1</sup> M. Jahnátek, J. Hafner, and M. Krajčí, Phys. Rev. B **79**, 224103 (2009).

<sup>2</sup> D. M. Clatterbuck, D. C. Chrzan, and J. W. Morris Jr., Acta Mater. **51**, 2271 (2003).

<sup>3</sup> A. Kelly and N. H. Macmillan, *Strong Solids* (Clarendon, Oxford, 1986).

<sup>4</sup> M. Yoshida, T. Sumomogi, T. Endo, H. Maeta, and T. Kino, Mater. Trans. **48**, 1 (2007).

<sup>5</sup> M. Černý, M. Šob, J. Pokluda, and P. Šandera, J. Phys.: Condens. Matter **16**, 1045 (2004).

<sup>6</sup> N. Nagasako, M. Jahnátek, R. Asahi, and J. Hafner, Phys. Rev. B **81**, 094108 (2010).

<sup>7</sup> Y. J. Wang and C. Y. Wang, Appl. Phys. Lett. **94**, 261909 (2009).

<sup>8</sup> M. Šob, L. G. Wang, and V. Vitek, Mater. Sci. Eng., A **234-236**, 1075 (1997).

- <sup>9</sup> W. Li and T. Wang, Phys. Rev. B **59**, 3993 (1999).
- <sup>10</sup> Y. Umeno and T. Kitamura, Mater. Sci. Eng. B **88**, 79 (2002).
- <sup>11</sup> K. Yashiro, M. Oho, and Y. Tomita, Comp. Mater. Sci. **49**, 397 (2004).
- <sup>12</sup> H. B. Zhou, Y. Zhang, Y. L. Liu, M. Kohyama, P. G. Yin, and G. H. Lu, J. Phys.: Condens. Matter **21**, 175407 (2009).
- <sup>13</sup> A. T. Paxton, P. Gumbsch, and M. Methfessel, Phil. Mag. Lett. **63**, 267 (1991).
- <sup>14</sup> D. Roundy, C. R. Krenn, M. L. Cohen, and J. W. Morris, Jr., Phys. Rev. Lett. **82**, 2713 (1999).
- <sup>15</sup> W. D. Luo, D. Roundy, M. L. Cohen, and J. W. Morris, Jr., Phys. Rev. B **66**, 094110 (2002).
- <sup>16</sup> D. Roundy, C. R. Krenn, M. L. Cohen, and J. W. Morris, Jr., Philos. Mag. A **81**, 1725 (2001).
- <sup>17</sup> C. R. Krenn, D. Roundy, J. W. Morris, Jr., and M. L. Cohen, Mater. Sci. Eng. A **319-321**, 111 (2001).
- <sup>18</sup> M. Černý and J. Pokluda, Phys. Rev. B **82**, 174106 (2010).
- <sup>19</sup> T. S. Li, J. W. Morris Jr., N. Nagasako, S. Kuramoto, and D. C. Chrzan, Phys. Rev. Lett. **98**, 105503 (2007).
- <sup>20</sup> H. M. Chung, B. A. Loomis, and D. L. Smith, J. Nucl. Mater. **239**, 139 (1996).
- <sup>21</sup> H. Matsui, K. Fukumoto, D. L. Smith, H. M. Chung, W. van Witzenburg, and S. N. Votinov, J. Nucl. Mater. **233**, 92 (1996).
- <sup>22</sup> D. L. Smith, H. M. Chung, H. Matsui, and A. F. Rowcliffe, Fusion Eng. Des. **41**, 7 (1998).
- <sup>23</sup> R. J. Kurtz, K. Abe, V. M. Chernov, V. A. Kazakov, G. E. Lucas, H. Matsui, T. Muroga, G. R. Odette, D. L. Smith, and S. J. Zinkle, J. Nucl. Mater. **283**, 70 (2000).
- <sup>24</sup> D. L. Smith, M. C. Billone, and K. Natesan, Int. J. Refract. Met. Hard Mater. **18**, 213 (2000).
- <sup>25</sup> T. Muroga, T. Nagasaka, K. Abe, V. M. Chernov, H. Matsui, D. L. Smith, Z. Y. Xu, and S. J. Zinkle, J. Nucl. Mater. **307**, 547 (2002).
- <sup>26</sup> H. M. Chung, B. A. Loomis, and D. L. Smith, J. Nucl. Mater. **212**, 804 (1994).
- <sup>27</sup> K. Natesan, W. K. Soppet, and M. Uz, J. Nucl. Mater. **258**, 1476 (1998).
- <sup>28</sup> D. S. Gelles, P. M. Rice, S. J. Zinkle, and H. M. Chung, J. Nucl. Mater. **258**, 1380 (1998).
- <sup>29</sup> H. M. Chung and D. L. Smith, J. Nucl. Mater. **258**, 1442 (1998).
- <sup>30</sup> E. G. Donahue, G. R. Odette, and G. E. Lucas, J. Nucl. Mater. **283**, 518 (2000).
- <sup>31</sup> P. M. Rice and S. J. Zinkle, J. Nucl. Mater. **258**, 1414 (1998).
- <sup>32</sup> X. Q. Li, H. L. Zhang, S. Lu, W. Li, J. J. Zhao, B. Johansson, and L. Vitos, Phys. Rev. B **86**, 014105 (2012).
- <sup>33</sup> X. Q. Li, C. Zhang, J. J. Zhao, and B. Johansson, Comp. Mater. Sci. **50**, 2727 (2011).
- <sup>34</sup> P. Hohenberg and W. Kohn, Phys. Rev. B **136**, 864 (1964).
- <sup>35</sup> J. P. Perdew, K. Burke, and M. Ernzerhof, Phys. Rev. Lett. **77**, 3865 (1996).
- <sup>36</sup> O. K. Andersen, O. Jepsen, and G. Krier, in *Lectures on Methods of Electronic Structure Calculations*, edited by V. Kumar, O. K. Andersen, and A. Mookerjee (World Scientific, Singapore, 1994) p. 63.
- <sup>37</sup> L. Vitos, Phys. Rev. B **64**, 014107 (2001).
- <sup>38</sup> L. Vitos, H. L. Skriver, B. Johansson, and J. Kollár, Comput. Mater. Sci. **18**, 24 (2000).
- <sup>39</sup> B. L. Gyorffy, Phys. Rev. B **5**, 2382 (1972).
- <sup>40</sup> A. Taga, L. Vitos, B. Johansson, and G. Grimvall, Phys. Rev. B **71**, 014201 (2005).
- <sup>41</sup> L. Vitos, I. A. Abrikosov, and B. Johansson, Phys. Rev. Lett. **87**, 156401 (2001).
- <sup>42</sup> L. Vitos, *Computational Quantum Mechanics for Materials Engineers* (Springer-Verlag, London, 2007).
- <sup>43</sup> L. Huang, L. Vitos, S. K. Kwon, B. Johansson, and R. Ahuja, Phys. Rev. B **73**, 104203 (2006).
- <sup>44</sup> J. Zander, R. Sandström, and L. Vitos, Comput. Mater. Sci. **41**, 86 (2007).
- <sup>45</sup> B. Magyari-Köpe, G. Grimvall, and L. Vitos, Phys. Rev. B **66**, 064210 (2002).
- <sup>46</sup> B. Magyari-Köpe, L. Vitos, and G. Grimvall, Phys. Rev. B **70**, 052102 (2004).
- <sup>47</sup> L. Vitos, P. A. Korzhavyi, and B. Johansson, Nat. Mater. **2**, 25 (2003).
- <sup>48</sup> V. Ozoliņš, C. Wolverton, and A. Zunger, Phys. Rev. B **57**, 4816 (1999).
- <sup>49</sup> E. C. Bain, Trans. AIME **70**, 25 (1924).
- <sup>50</sup> F. Milstein, H. E. Fang, and J. Marschall, Phil. Mag. A **70**, 621 (1994).
- <sup>51</sup> C. Kittel, *Introduction to Solid State Physics*, Vol. 23 (Wiley, New York, 1986).
- <sup>52</sup> D. I. Bolef, R. E. Smith, and J. G. Miller, Phys. Rev. B **3**, 4100 (1971).
- <sup>53</sup> D. O. Van Ostenburg, D. J. Lam, H. D. Trapp, and D. E. McLeod, Phys. Rev. **128**, 1550 (1962).
- <sup>54</sup> G. Grimvall, *Thermophysical Properties of Materials* (North-Holland, Amsterdam, 1999).
- <sup>55</sup> Y. L. Liu, H. B. Zhou, and Y. Zhang, J. Nucl. Mater. **416**, 345 (2011).
- <sup>56</sup> M. Jahnátek, M. Krajčí, and J. Hafner, Phys. Rev. B **71**, 024101 (2005).
- <sup>57</sup> K. D. Joshi and S. C. Gupta, High Pressure Res. **27**, 259 (2007).
- <sup>58</sup> N. Nagasako, M. Jahnátek, R. Asahi, and J. Hafner, Phys. Rev. B **81**, 094108 (2010).
- <sup>59</sup> J. Frenkel, Z. Phys. **7**, 323 (1926).
- <sup>60</sup> E. Orowan, Rep. Prog. Phys. **12**, 185 (1949).
- <sup>61</sup> Y. L. Liu, Y. Zhang, R. J. Hong, and G. H. Lu, Chin. Phys. B **18**, 1923 (2009).
- <sup>62</sup> M. Šob, L. G. Wang, and V. Vitek, Phil. Mag. B **78**, 653 (1998).
- <sup>63</sup> M. Černý and J. Pokluda, Phys. Rev. B **76**, 024115 (2007).
- <sup>64</sup> H. L. Skriver, Phys. Rev. B **31**, 1909 (1985).
- <sup>65</sup> A. T. Paxton, M. Methfessel, and H. M. Polatoglou, Phys. Rev. B **41**, 8127 (1990).
- <sup>66</sup> P. J. Craievich, M. Weinert, J. M. Sanchez, and R. E. Watson, Phys. Rev. Lett. **72**, 3076 (1994).
- <sup>67</sup> P. M. Marcus, F. Jona, and S. L. Qiu, Phys. Rev. B **66**, 064111 (2002).
- <sup>68</sup> M. Šob, M. Friák, D. Legut, J. Fiala, and V. Vitek, Mat. Sci. Eng. A **387-389**, 148 (2004).
- <sup>69</sup> S. Schönecker, *Theoretical Studies of Epitaxial Bain Paths of Metals*, Ph.D. thesis, TU Dresden, Germany (2011).
- <sup>70</sup> J. W. Morris Jr., C. R. Crenn, D. Roundy, and M. L. Cohen, in *Phase Transformations and Evolution in Materials*, edited by P. E. A. Turchi and A. Gonis (The minerals, metals & materials society, 2000) p. 187.
- <sup>71</sup> K. W. Katahara, M. H. Manghnani, and E. S. Fisher, J. Phys. F **9**, 773 (1979).
- <sup>72</sup> D. I. Bolef, R. E. Smith, and J. G. Miller, Phys. Rev. B **3**, 4100 (1971).

- <sup>73</sup> S. N. Votinov, M. I. Solonin, Y. I. Kazennov, V. P. Konratjev, A. D. Nikulin, V. N. Tebus, E. O. Adamov, S. E. Bougaenko, Y. S. Strebkov, A. V. Sidorenkov, V. B. Ivanov, V. A. Kazakov, V. A. Evtikhin, I. E. Lyublinski, V. M. Trojanov, A. E. Rusanov, V. M. Chernov, and G. A. Birgevoj, *J. Nucl. Mater.* **233-237**, 370 (1996).
- <sup>74</sup> J. Friedel, "The physics of metals: 1. Electrons," (Ziman, M. J., Ed., Cambridge University Press, London, 1969) Chap. 8: Transition Metals. Electronic Structure of the *d*-band. Its Role in the Crystalline and Magnetic Structures.
- <sup>75</sup> D. G. Pettifor, "A quantum-mechanical critique of the Miedema rules for alloy formation," (Academic Press, Inc., 1987) pp. 43–92.
- <sup>76</sup> W. A. Harrison, *Electronic Structure and the Properties of Solids: the Physics of the Chemical Bond*, 2nd ed. (Dover Publications, Inc., 1989).
- <sup>77</sup> D. G. Pettifor, *Bonding and Structure of Molecules and Solids* (Oxford University Press, Oxford, 1995).
- <sup>78</sup> V. L. Moruzzi, A. R. Williams, and J. F. Janak, *Phys. Rev. B* **15**, 2854 (1977).
- <sup>79</sup> C. D. Gelatt, Jr., H. Ehrenreich, and R. E. Watson, *Phys. Rev. B* **15**, 1613 (1977).
- <sup>80</sup> V. L. Moruzzi and P. M. Marcus, *Phys. Rev. B* **48**, 7665 (1993).
- <sup>81</sup> P. Söderlind, O. Eriksson, J. M. Wills, and A. M. Boring, *Phys. Rev. B* **48**, 5844 (1993).
- <sup>82</sup> J. M. Wills, O. Eriksson, P. Söderlind, and A. M. Boring, *Phys. Rev. Lett.* **68**, 2802 (1992).
- <sup>83</sup> O. K. Andersen, O. Jepsen, and D. Glötzel, "Highlights of condensed-matter physics," (North-Holland, Bassani, F., Fumi, F., and Tossi, M. P., Eds., Amsterdam, 1985) Chap. Canonical description of the band structure of metals, pp. 59–176.
- <sup>84</sup> M. Zelený, M. Friák, and M. Šob, *Phys. Rev. B* **83**, 184424 (2011).
- <sup>85</sup> L. G. Wang, M. Šob, and Z. Y. Zhang, *J. Phys. Chem. Solids* **64**, 863 (2003).